ENHANCED LIGHT ABSORPTION IN THIN-FILM SILICON SOLAR CELLS BY SCATTERING FROM EMBEDDED DIELECTRIC NANOPARTICLES

James R. Nagel[1] and Michael A. Scarpulla[1]
[1]Department of Electrical and Computer Engineering, University of Utah, Salt Lake City, Utah, USA

ABSTRACT

We investigate the light-trapping effects of dielectric nanoparticles embedded within the active semiconductor layer of a thin-film solar cell. The baseline model consists of a 1.0 μm slab of crystalline silicon on an aluminum back contact topped with a 75 nm Si_3N_4 anti-reflective coating. Using finite-difference time-domain (FDTD) simulations, we calculate the absorption gain due to a periodic array of SiO_2 nanospheres with characteristic depth, diameter, and pitch. Under optimal conditions, spectrally integrated absorption gain due to embedded spheres can reach as high as 23.4 % relative to the baseline geometry. Using a geometry with an Au-core and SiO_2 shell, it is even possible to reach 30 % after accounting for Ohmic losses. We also discuss the trade-offs between broadband scattering efficiency, poor absorption at long-wavelengths, and semiconductor displacement due to the embedded nanospheres.

INTRODUCTION

Photovoltaic power generation holds great promise for satisfying our future needs for renewable energy, but still continues to struggle for a cost-competitive edge at industrial-scale manufacture. Crystalline silicon (c-Si) is an especially promising candidate for this role because it is abundant, non-toxic, possesses a nearly ideal bandgap, and is well-established in the semiconductor industry for large-scale production. Yet despite these advantages, the material and processing costs associated with traditional wafer-based designs account for large fractions of the total manufacturing expense. Thin-film technology therefore seeks to reduce the usual 100-200 μm wafer thickness down to 1.0 μm or less. Unfortunately, the absorption length for c-Si is on the order of many tens of microns over much of the visible spectrum, thereby limiting the absorption efficiency of thin silicon films. So despite their recent commercial growth, the efficiency of thin-film silicon photovoltaics has currently not yet exceeded 10-12 % [1], thus leaving much room for improvement.

To help alleviate the low efficiency of thin film cells, significant research effort has been directed toward ways to improve the light-trapping properties of such devices. This typically involves some type of scheme for laterally scattering light within the active layers of the cell, thereby increasing the optical path length of propagation for normally-incident waves. For example, surface texturing is an effective tool that has been demonstrated via etched pyramids [2] and random roughness [3]. Plasmonic nanoparticles placed along the surface of the cell have likewise demonstrated light-trapping properties [4]. However, for the case of ultra-thin films on the order of 1.0 μm, many of these schemes may be impractical to commercially implement. For example, surface texturing tends to increase surface recombination and sheet resistivity of a photovoltaic cell. Often times, the necessary feature size of the texturing itself may even exceed the film thickness.

In a recent publication [5], we introduced a concept for light trapping by using wavelength-scale dielectric nanoparticles embedded directly within the active semiconductor layer. Through numerical simulation, we showed that light injection from an anti-reflective coating (ARC) is virtually unaffected by the presence of embedded scatterers underneath, thereby decoupling the ARC from light trapping schemes and allowing independent optimization of both. Scattering light inside the high-index Si allows access to more of the optical modes inside the absorber, thus pushing closer to the ergodic efficiency limit. This concept has also been used experimentally to demonstrate a 16 % gain in short-circuit current density by embedding spherical SiO_2 nanospheres in a tandem solar cell made from crystalline and amorphous silicon [6].

In this work, we expand on our previous analysis by considering a photovoltaic cell with finite thickness and an aluminum back contact. This introduces waveguiding effects that were absent in our earlier work. All simulation data were generated using commercial FDTD-based software [7]. We also caution that careful corrections must be made to account for the program's incorrect interpolation of the tabulated extinction coefficient for Si at long wavelengths.

BASELINE SOLAR CELL MODEL

Depicted in Figure 1(a), the baseline cell consists of a 1.0 μm slab of c-Si with an aluminum back-contact. At the surface of the c-Si layer is a 75 nm slab of Si_3N_4 to serve as the ARC. Periodic boundary conditions were placed at the x- and y-boundaries to mimic the effects of an infinitely periodic unit cell. A perfectly-matched layer (PML) was placed 400 nm above the ARC in order to absorb reflected energy at the top boundary. Because the skin-depth of aluminum is less than 50 nm over the entire visible spectrum, a perfect electrical conductor (PEC) boundary was placed 200 nm below the back contact interface to remove the computational complexity of an extra PML. We also neglected the effects of doping on the dielectric properties of the c-Si layer, which are insignificant in the context of this work for wavelengths below 1200 nm.

The output of interest from our simulations is the absorption factor A(λ) defined as the fraction of incident power that is absorbed within the c-Si layer at a specified

978-1-4244-9965-6/11/$26.00 ©2011 IEEE

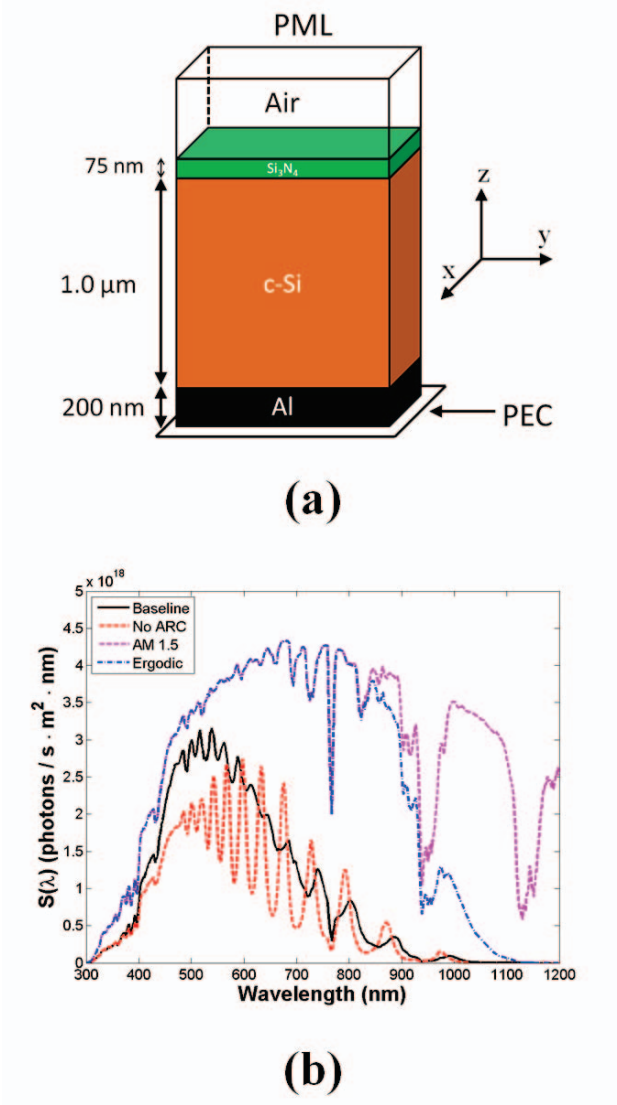

Figure 1: (a) Baseline solar cell simulation model. The FDTD boundary conditions are periodic along x and y, mimicking an infinite array of cells. (b) S(λ) computed by the simulation model. Also shown is the AM 1.5 spectrum, the ergodic limit, and S(λ) for an equivalent cell with no ARC.

free-space excitation wavelength λ. For an ideal PV cell, A(λ) would be unity across the entire solar spectrum, though physical restrictions prevent this. For example, the ergodic limit introduced by Yablonovitch and Cody [8] is a common benchmark that assumes zero surface reflectance, zero back transmittance, isotropic scattering at each interface, and low loss in the absorbing medium. Under these conditions, the maximum optical path-length of a slab of thickness w reaches a value of $\ell = 4n^2w$, with n being the real part of the wavelength-dependent index of refraction for the c-Si layer. Consequently, the ergodic limit for the absorption factor of a thin silicon film is

$$A(\lambda) = 1 - e^{-\alpha(\lambda)\ell(\lambda)}, \quad (1)$$

where the attenuation coefficient of silicon is given by $\alpha(\lambda) = 4\pi\kappa(\lambda)/\lambda$, with $\kappa(\lambda)$ being the extinction coefficient.

Once the absorption factor is determined for a given model, the primary figure of merit is the solar flux absorbance S(λ). This is defined as the absorption factor weighted by the AM 1.5 photon flux $\Phi_0(\lambda)$ [9]:

$$S(\lambda) = A(\lambda)\Phi(\lambda), \quad (2)$$

where $\Phi_0(\lambda)$ has units of photons·s^{-1}·m^2·nm^{-1}. The short-circuit current density J_{sc} is therefore related to the integral of S(λ) times the internal quantum efficiency IQE(λ):

$$J_{sc} = q\int_0^\infty S(\lambda)\mathrm{IQE}(\lambda)d\lambda, \quad (3)$$

with q being the electron charge. Thus, if the IQE were a known function, any simulation output could be used to compute J_{sc} under ideal AM 1.5 illumination. However, since the IQE is cell-specific, this paper is limited to photon capture only, which is equivalent to calculating J_{sc} under the assumption that IQE = 1 over all wavelengths. This parameter is therefore referred to as the spectrally-integrated photon absorption efficiency, or IAE for short [10].

An example simulation output for the baseline geometry is depicted in Figure 1(b) using dielectric functions taken from sampled data in [11]. Using analytical calculations based on light transmission through a series of planar dielectric boundaries [12], we have also verified that the simulation error is < 1% for this model. For reference, we plot the incident AM 1.5 photon flux as well as the ideal absorbance that would occur at the ergodic limit. Because the bandgap for silicon occurs at λ_{Gap} = 1130 nm and there are few photons below 300 nm, we limit our spectrum of interest to 300-1200 nm.

Assuming perfect IQE, the IAE for the baseline cell is only 41 % of the ergodic limit for a 1.0 µm cell (note the strong thickness dependence of IAE). This illustrates the untapped efficiency of simplistic thin-film designs due to poor light management. Another important feature is the dramatic decline in the ergodic absorption limit at wavelengths above 900 nm. This behavior is due to the low absorption coefficient α(λ) of the Si indirect bandgap. Consequently, although very large enhancements in path length are possible for such long wavelengths, the amount of actual J_{SC} recoverable even in the ergodic limit for such thin solar cells is small compared to the recoverable J_{SC} at shorter wavelengths. Thus we break from conventional

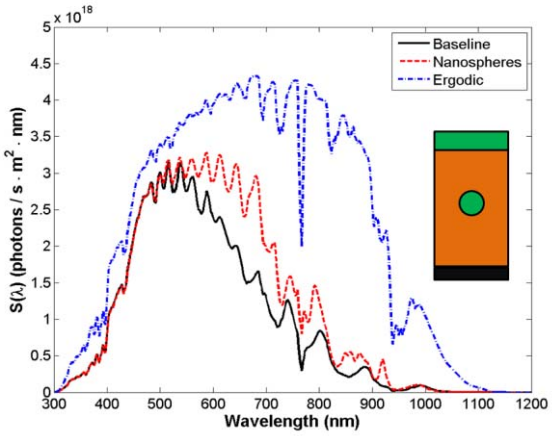

Figure 2: Absorption spectrum for D = 200 nm, z_0 = 450 nm, and p = 375 nm. Total absorption gain due to the embedded nanoparticle array is 23.4 %

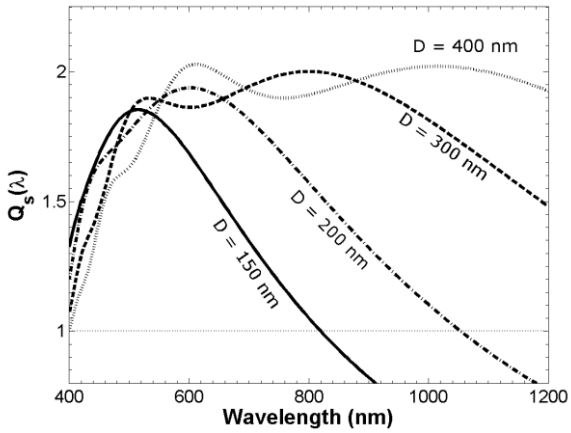

Figure 3: (a) Scattering efficiencies for spheres of SiO2 embedded in c-Si. Indicated wavelengths are in free-space units.

wisdom in suggesting that an efficient light-management scheme for such thin cells should be optimized not for Si band edge photons but for those of shorter wavelength.

For comparison, we also include the absorbance spectrum of an equivalent c-Si layer with no ARC placed on top. Without the ARC, the absorbance curve exhibits strong peaks and valleys, which are characteristic of Fabry-Perot resonances. Most importantly, the IAE is 26 % less than the same cell with the ARC. This illustrates the significant value of a simple ARC, and any practical light-trapping scheme should strive to be competitive with this baseline level of efficiency.

EMBEDDED DIELECTRIC NANOSPHERES

The experimental solar cell is identical to the baseline, but with a spherical SiO_2 nanoparticle embedded within the active c-Si layer. The sphere is defined by a specific depth z_0 below the c-Si surface, a diameter D, and a pitch p of the repeating array. As a demonstration case, Figure 2 plots S(λ) for a D = 200 nm sphere at depth z_0 = 450 nm, and a pitch of p = 375 nm. These parameters represent nearly optimal values for light-trapping derived from the analysis in this paper. For reference, the baseline cell is also plotted to emphasize the increase in absorption that occurs across the solar spectrum. The resultant absorption gain is due solely to the increased path-length of the radiation as it scatters off the embedded nanoparticles and couples into guided or weakly radiating modes within the cell. Numerical integration of the two curves yields a 23.4 % gain in the IAE due to the presence of the embedded nanoparticles.

Although the choice of material for the embedded nanoparticles is somewhat arbitrary, we have opted to investigate SiO_2 for several advantageous reasons. Not only is SiO_2 optically lossless over the entire solar spectrum, but under the right circumstances the Si/SiO_2 interface can have low dangling bond densities. This may allow SiO_2 nanospheres to be embedded within the cell without significantly contributing to deleterious recombination loss, especially in the case of tandem or multi-junction cells where recombination is actually required for the efficient operation of the connecting tunnel junctions. The dielectric contrast between SiO_2 ($n \approx 1.5$) and c-Si ($n \approx 3.5$) is also reasonably high, thereby leading to strong light scattering by the embedded particles. If we further limit ourselves to spherical geometry, then classical Mie theory provides closed-form analytical expressions for describing this interaction [13]. For the case of a lossy ambient medium like Si, advanced formulations incorporating the complex dielectric constants are also available for accurate calculations of scattering efficiency [14]. Significant differences appear primarily below 500 nm for Si, where κ is a significant fraction of the real index n.

Mie calculations for spherical particles of SiO_2 embedded in c-Si are summarized in Figure 3 for varying particle diameters. The key behavior appears to be that large spheres possess a more broadband scattering efficiency than small spheres, but that scattering efficiency also saturates around a maximum value of $Q_s \approx 2$.

Although we have assumed a perfectly periodic lattice in our simulation models, such a feature is not essential for absorption gain in a real device. Whether scattering is coherent or not, any feature that redirects the incident radiation away from normal propagation must generally result in a subsequent path-length enhancement. Consequently, we expect to see significant absorption gains whether the embedded particles are ordered or disordered.

PARAMETRIC SWEEPS

Figure 4 summarizes a series of simulations by sweeping through each set of design parameter. Figure 4(a) begins with a D = 200 nm sphere at a fixed pitch of p = 400 nm and sweeps the depth from top to bottom within the c-Si layer. Figure 4(b) fixes the depth at z_0 = 500 nm and varies the diameter. The pitch is also varied according to p = 2D in order to maintain a fixed area coverage of embedded particles. Figure 4(c) varies the pitch with D = 200 nm and z_0 = 500 nm.

The depth sweep of Figure 4(a) indicates that an embedded sphere is best placed away from the back contact of the cell. This behavior can be understood in terms of light scattering by a spherical particle near a conducting planar boundary [15]. It is known that light scattering is heavily attenuated for a sphere placed directly adjacent to the boundary but grows as the particle is moved further away. However, because c-Si is a lossy material, such gains in scattering efficiency eventually diminish with distance since the particle no longer couples efficiently with its image inside the conducting plane. Consequently, there is an ideal placement near z_0 = 450 nm that optimizes these two trade-offs within the cell.

The diameter sweep of Figure 4(b) shows us another trade-off between competing physical effects. As shown in Figure 3, the scattering efficiency of SiO_2 spheres embedded in c-Si saturates around a value of Q_s = 2, and merely grows more broadband as diameter increases. However, as mentioned before, light scattering above λ = 1000 nm produces little gain in the IAE for a 1.0 μm-thick cell since c-Si is such a poor absorber in this regime. Consequently, large spheres merely displace more active material without significantly contributing to the overall IAE. This causes a steady decline in absorption gain for particles larger than a diameter of 175-200 nm.

In the final series shown in Figure 4(c), we can see a clear transition between sparse array behavior versus dense arrays where multiple scattering is relevant. For $p\alpha(\lambda) >> 1$, the amplitudes of both radiation modes and guided modes will have significantly decayed by the time they encounter any neighboring scatterers, thereby minimizing the importance of multiple scattering. As a consequence, each embedded particle acts in isolation from all other particles, and gain in IAE is approximately linear with the area coverage. If we further note that area coverage is defined by $\pi r^2/p^2$, then asymptotic gain in IAE may be expressed as

$$G = C\frac{\pi r^2}{p^2}, \qquad (p\alpha(\lambda) >> 1) \tag{4}$$

where C ≈ 0.98 is a scale factor that must be empirically determined from the data. A large value for C implies very

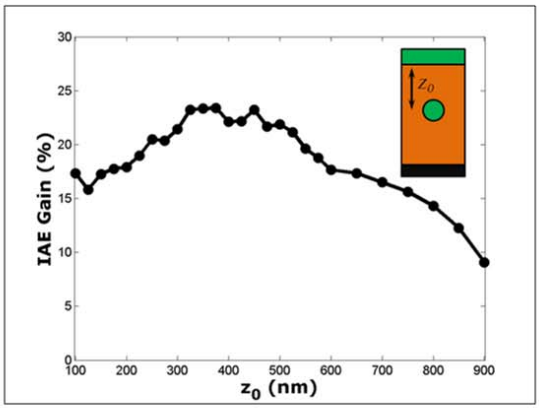

(a)

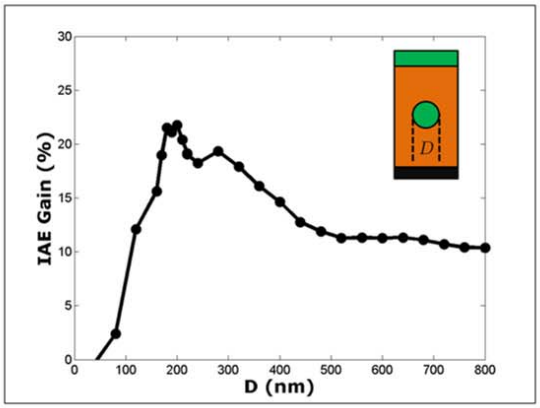

(b)

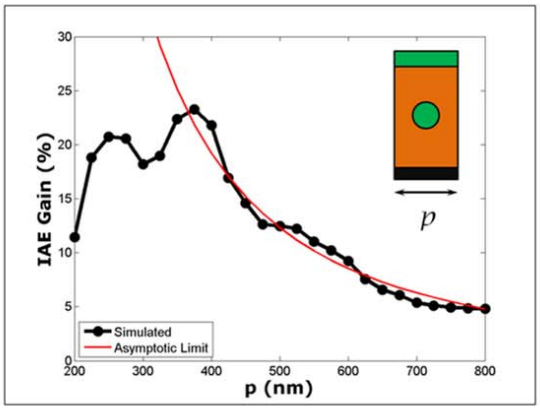

(c)

Figure 4: Parametric sweeps of (a) particle height with D = 200 nm and p = 400 nm, (b) particle diameter with z_0 = 500 nm and p = 2D, and (c) array pitch with D = 200 nm and z_0 = 500 nm.

strong scattering by individual particles, while a small value implies very weak scattering. This curve is superimposed into Figure 4(c) to demonstrate the limiting behavior at large array pitches.

When the spheres are brought close together, multiple scattering becomes important. For weakly radiating modes, this can lead to greater coupling into the desirable guided modes and yield greater IAE. However, the same scattering centers also couple back into radiation modes, thereby reducing the IAE. The dominance of each case depends heavily on array pitch, and even the mode structure of the waveguide formed by the Si layer. Such behavior is likewise present in the other two data sets and contributes to a small degree of chaotic variation on top of any general trends. For very closely-packed arrays, the displacement of active material also becomes a significant factor that contributes to a net decline in the IAE.

AU CORE WITH SIO_2 SHELL

One of the fundamental limitations to absorption gain with SiO_2 nanospheres is governed by their finite scattering efficiency when embedded in c-Si. More conductive materials like Au and Ag possess a much stronger dielectric contrast with c-Si and can therefore exert a greater influence on incident radiation. However, metallic spheres embedded within a photovoltaic cell will certainly lead to severe recombination loss and offset any potential efficiency gains due to light absorption. A potential compromise is to therefore coat the metallic spheres with a thin layer of dielectric insulation, thereby retaining strong scattering efficiency while simultaneously protecting against recombination. Such core-shell nanoparticles are readily grown in solution [16], thus making such designs feasible.

The geometry of an embedded core/shell nanoparticle is defined by the same parameters as before, but with a shell thickness t surrounding the core. Figure 5 summarizes the scattering efficiency Q_s of an Au-core nanosphere with core diameter D = 200 nm and an SiO_2 shell of varying thickness. These values were computed using standard Mie theory for a core-shell structure in a lossless ambient medium [13], which is approximately valid for c-Si at wavelengths above 500 nm. Although a bare Au sphere embedded in c-Si is an excellent scatterer over much of the visible spectrum, it is readily apparent that even a thin 10 nm shell of SiO_2 is enough to completely negate the enhanced scattering properties of the core. However, it is also important for the dielectric shell to possess sufficient thickness in order to serve as a reliable barrier against recombination loss. We therefore chose to explore a thickness of t = 5 nm as a reasonable compromise between these two design parameters.

Figure 6 summarizes the gain in IAE using a D = 200 nm Au core with a 5 nm SiO_2 shell. The particle depth was set to z_0 = 450 nm with an array pitch of p = 375 nm. Very

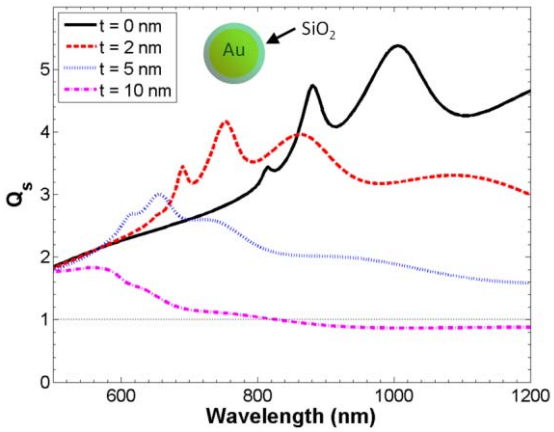

Figure 5: Scattering efficiency of a core/shell nanosphere embedded in lossless c-Si under varying shell thicknesses. The Au core has a diameter D = 200 nm.

importantly, because the Au core is conductive, we subtract the Ohmic losses within the nanosphere when computing the IAE. Even after accounting for this absorption inside the core, the gain in IAE was 30.5 %. This serves to indicate the further light-trapping potential of embedded nanoparticles with greater scattering efficiencies.

CONCLUSIONS

This paper explores the gain in spectrally integrated absorption efficiency of a 1.0 μm silicon solar cell due to the presence of embedded dielectric nanospheres. We have shown that absorption gain can reach as high as 23 % under ideal conditions, and can even push beyond 30 % when using a core/shell particle of Au/SiO_2. This behavior is due to the optical path-length enhancement that occurs from coupling into the guided modes of the ultra-thin 1 μm c-Si cell structure. We also inferred a series of design principles from our data that account for trade-offs between such factors as scattering efficiency, displacement of active semiconductor material, silicon absorption at long wavelengths, and mode coupling. The ideal height placement was found to be within a range of 400-500 nm, which represents a near-ideal interaction between the embedded particles and their images within the Al back contact. The ideal diameter was found to be within 175-250 nm, which is governed by the trade-offs between broadband scattering efficiency, poor absorption at long wavelengths, and semiconductor displacement. Finally, the ideal array pitch fell within 375-400 nm, which provides the greatest particle density before gain in IAE strongly deviates from the ideal $1/p^2$ trend. It is our hope that these principles will prove helpful in experimental work into the nature of light-trapping via embedded dielectric nanoparticles.

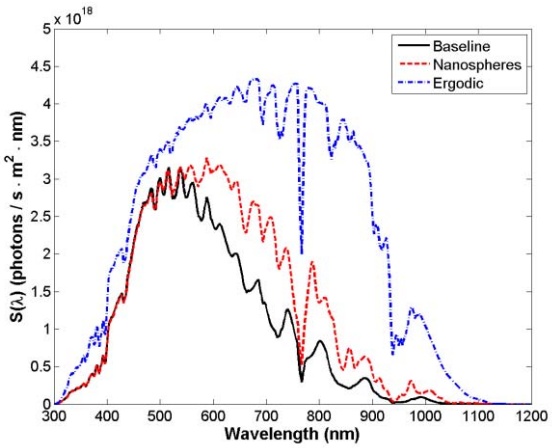

Figure 6: S(λ) for the Au-core/SiO_2-shell embedded in the baseline cell. D = 200 nm, t = 5 nm, p = 375 nm, and z_0 = 450 nm. Gain in IAE is 30.5 %.

REFERENCES

[1] J. Schmidtke, "Commercial status of thin-film photovoltaic devices and materials," *Opt. Express*, **18**, 2010, pp. 477-486

[2] P. Campbell and M. A. Green, "Light trapping properties of pyramidally textured surfaces," *J. of Appl. Phys.*, **62**, 1987, pp. 243-249

[3] S. Koynov, M. S. Brandt, and M. Stutzmann, "Black nonreflecting silicon surfaces for solar cells," *Appl. Phys. Lett.*, **88**, 2006, p. 203017

[4] H. A. Atwater and A. Polman, "Plasmonics for improved photovoltaic devices," *Nat. Mater.*, **9**, 2010, pp. 205–213.

[5] J. R. Nagel and M. A. Scarpulla, "Enhanced absorption in optically thin solar cells by scattering from embedded dielectric nanoparticles," *Opt. Express*, **18**, 2010, pp. A139–A146.

[6] S. Nunomura, A. Minowa, H. Sai, and M. Kondo, "Mie scattering enhanced near-infrared light response of thin-film silicon solar cells," *Appl. Phys. Lett.*, **97**, no. 6, 2010, p. 063507.

[7] Lumerical Solutions, Inc., http://www.lumerical.com/

[8] E. Yablonovitch and G. D. Cody, "Intensity enhancement in texture optical sheets for solar cells," *IEEE Trans. Electron Devices*, **29**, 1982, pp. 300–305.

[9] http://rredc.nrel.gov/solar/spectra/am1.5/

[10] P. N. Saeta, V. E. Ferry, D. Paci_ci, J. N. Munday, and H. A. Atwater, "How much can guided modes enhance absorption in thin solar cells," *Opt. Express*, **17**, 2009, pp. 20975-20990.

[11] E. D. Palik, Ed., *Handbook of Optical Constants of Solids*. Academic Press, 1998.

[12] J. A. Kong, *Electromagnetic Wave Theory*, Cambridge, MA: EMW Publishing, 2000.

[13] C. F. Bohren and D. R. Huffman, *Absorption and Scattering of Light by Small Particles*, Wiley, 1983.

[14] I. W. Sudiarta and P. Chylek, "Mie-scattering formalism for spherical particles embedded in an absorbing medium," J. Opt. Soc. Am. A, **18**, 2001, pp. 1275-1278.

[15] B. R. Johnson, "Light scattering from a spherical particle on a conducting plane: I. normal incidence," *J. Opt. Soc. Am. A*, **9**, 1992, pp. 1341-1351

[16] L. M. Liz-Marzan, M. Giersig, and P. Mulvaney, "Synthesis of nanosized gold-silica core-shell particles," *Langmuir*, **12**, 1996 pp. 4329-4335.